

ISSN: 0095-8972 (Print) 1029-0389 (Online) Journal homepage: <http://www.tandfonline.com/loi/gcoo20>


Syntheses, crystal structures, spectroscopy, electrochemical and magnetic properties of four cyanido-bridged $M^{II}-Mn^{III}$ ($M = Fe, Ru, Os$) complexes

Yong Wang, Xiao Ma, Shengmin Hu, Zhenzhen Xue, Yuehong Wen, Tianlu Sheng & Xintao Wu

To cite this article: Yong Wang, Xiao Ma, Shengmin Hu, Zhenzhen Xue, Yuehong Wen, Tianlu Sheng & Xintao Wu (2015) Syntheses, crystal structures, spectroscopy, electrochemical and magnetic properties of four cyanido-bridged $M^{II}-Mn^{III}$ ($M = Fe, Ru, Os$) complexes, Journal of Coordination Chemistry, 68:1, 55-70, DOI: [10.1080/00958972.2014.981537](https://doi.org/10.1080/00958972.2014.981537)


To link to this article: <http://dx.doi.org/10.1080/00958972.2014.981537>

 View supplementary material 

 Accepted author version posted online: 27 Oct 2014.
Published online: 20 Nov 2014.

 Submit your article to this journal 

 Article views: 91

 View related articles 

 View Crossmark data 

 Citing articles: 2 View citing articles 

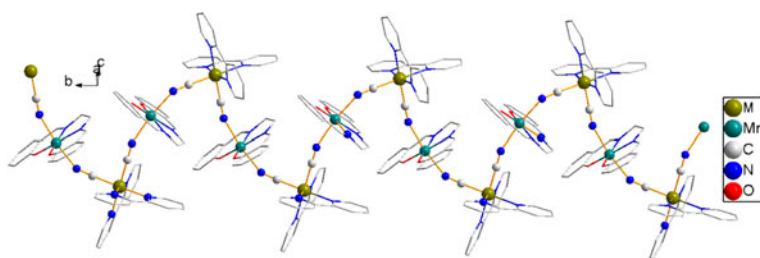
Syntheses, crystal structures, spectroscopy, electrochemical and magnetic properties of four cyanido-bridged M^{II} – Mn^{III} ($M = Fe, Ru, Os$) complexes

YONG WANG^{†‡}, XIAO MA[†], SHENGMIN HU[†], ZHENZHEN XUE^{†‡},
YUEHONG WEN[†], TIANLU SHENG^{*†} and XINTAO WU[†]

[†]State Key Laboratory of Structure Chemistry, Fujian Institute of Research on the Structure of Matter,
Chinese Academy of Sciences, Fuzhou, PR China

[‡]School of Chemistry and Chemical Engineering, University of Chinese Academy of Sciences,
Beijing, PR China

(Received 25 June 2014; accepted 30 September 2014)



Four paramagnetic cyanido-bridged 1-D heteronuclear zigzag chain complexes composed of M^{II} – CN – Mn^{III} ($M = Fe, Ru, Os$) were synthesized and fully characterized. The IR, electronic absorption spectral, electrochemical and magnetic properties of the complexes are discussed.

A family of paramagnetic cyanido-bridged 1-D heteronuclear zigzag chain isostructural complexes, [*cis*- M (bpy)₂(CN)₂Mn(salen)](PF₆) ($M = Fe$, **1**; $M = Ru$, **2**; $M = Os$, **3**; bpy = 2,2'-bipyridine, salen = N,N'-ethylenebis(salicylideneaminato)dianion) and [*cis*- Os (bpy)₂(CN)₂Mn(salcy)](PF₆) (**4**) (salcy = N,N'-(1,2-cyclohexanediyethylene) bis(salicylideneiminato)dianion), were synthesized by the reaction of diamagnetic precursors *cis*- M (bpy)₂(CN)₂ ($M = Fe, Ru, Os$) with paramagnetic Mn(III) Schiff bases, respectively. All these complexes were fully characterized by IR, MS, elemental analysis, and single-crystal X-ray diffraction. Electronic absorption spectral and electrochemical properties of **1–4** have also been measured. The temperature dependence of magnetic susceptibilities suggests that magnetic interactions in **1–4** are very weak and can be considered to have disappeared.

Keywords: Diamagnetic cyanido bridge; Mn-Schiff base; Osmium(II); Ruthenium(II); Iron(II)

*Corresponding author. Email: tsheng@fjirsm.ac.cn

1. Introduction

Numerous cyanide-bridged paramagnetic complexes have been synthesized and investigated for their various structures and magnetic functionalities such as room temperature magnets [1], single-molecule magnets (SMMs) [2], single-chain magnets (SCMs) [3], spin crossover (SCO) materials [4], and photo-magnetic materials [5]. Much effort in this field has been devoted to the study of the cyanide-bridged compounds in which paramagnetic metal ions are directly bridged by CN^- [6]. The magnetic chemistry of those polynuclear compounds with diamagnetic cyanide separating two magnetic centers has been paid much less attention. To date, only a few such examples have been reported [7].

Mn(III) complexes with N_2O_2 Schiff bases have strong uniaxial magnetic anisotropy created by the Jahn-Teller effect in an octahedral ligand field [8]. Hence, Mn-Schiff bases are good precursors in constructing cyanido-bridged magnetic materials [9]. Mn-Schiff bases maintain two accessible sites for incoming N- or O-donors in *trans*-positions. Thus, it would be reasonable to combine the blocked molecular precursors and the Mn-Schiff bases in pursuit of low-dimensional anisotropic molecular materials [10].

Recently, our group has investigated polynuclear compounds with a bridging diamagnetic cyanidometal ligand [11]. We have found that distant magnetic couplings across the diamagnetic cyanidometal centers are related to the configuration of the central metal [11b]. For example, *cis*-[Cp(dppe)Fe^{III}(μ -CN)Ru^{II}(bpy)₂(μ -CN)Fe^{III}(dppe)Cp][PF₆]₄ (dppe = 1,2-bis(diphenylphosphino ethane) is anti-ferromagnetic and *trans*-[Cp(dppe)Fe^{III}(μ -CN)Ru^{II}(bpy)₂(μ -CN)Fe^{III}(dppe)Cp][PF₆]₄ is ferromagnetic. In our previous reported compounds, the cyanide N-bonding metals are low spin. Furthermore, we would like to investigate magnetic coupling when the paramagnetic cyanide N-bonding metals are high spin. In this article, we report the syntheses, crystal structures, electronic absorption spectroscopy, electrochemical and magnetic properties of four new 1-D diamagnetic cyanido-bridged heteronuclear zigzag chain complexes [*cis*-M(bpy)₂(CN)₂Mn(salen)](PF₆) (M = Fe, **1**; M = Ru, **2**; M = Os, **3**) and [*cis*-Os(bpy)₂(CN)₂Mn(salcy)](PF₆) (**4**).

2. Experimental

2.1. Physical measurements

Elemental analyses (C, H, N) were carried out on a Vario MICRO elemental analyzer. Mass spectra (MS) were collected on DECAX-30000 LCQ Deca XP ion trap mass spectrometry using DMF (N,N-dimethylformamide) as the mobile phase. Infrared (IR) spectra were recorded on a Perkin-Elmer Spectrum One FT-IR spectrometer using KBr pellets. UV-vis spectra were measured on a PerkinElmer Lambda 900 UV-vis-NIR spectrophotometer. Electrochemical measurements were performed under argon using V3-Studio in acetonitrile solutions containing 0.1 M (Bu_4N)(PF₆) as a supporting electrolyte at a scan rate of 100 mV s⁻¹. Glassy graphite and platinum were used as working and counter electrodes, respectively, and the potentials were measured against a 3 M Ag/AgCl reference electrode. The magnetic susceptibilities of the crystalline samples were measured with a Magnetic Property Measurement System (MPMS) SQUID-XL under an applied magnetic field of 1000 Oe from 2 to 300 K. Diamagnetic corrections for **1-4** were made using Pascal's constants.

2.2. Materials and syntheses

All manipulations were performed under argon with the use of standard Schlenk techniques unless otherwise depicted. Dichloromethane and acetonitrile were dried by distillation over calcium hydride under argon. Methanol was dried by distillation over magnesium. DMF was dried by distillation over MgSO_4 . $\text{cis-Fe}(\text{bpy})_2(\text{CN})_2 \cdot 3\text{H}_2\text{O}$ [12], $\text{cis-Ru}(\text{bpy})_2(\text{CN})_2 \cdot 2\text{H}_2\text{O}$ [13], $\text{cis-Os}(\text{bpy})_2(\text{CN})_2 \cdot 2\text{H}_2\text{O}$ [14], $[\text{Mn}(\text{salen})(\text{H}_2\text{O})_2](\text{ClO}_4)$ [15], and $[\text{Mn}(\text{salcy})(\text{H}_2\text{O})_2](\text{ClO}_4)$ [16] were prepared according to the literature procedures. All other reagents were available commercially and used without purification.

2.3. Synthesis of $[\text{cis-Fe}(\text{bpy})_2(\text{CN})_2\text{Mn}(\text{salen})][\text{PF}_6]$ (**1**)

To a 25 ml methanol solution of $\text{cis-Fe}(\text{bpy})_2(\text{CN})_2 \cdot 3\text{H}_2\text{O}$ (100 mg, 0.211 mM), 1.1 equiv of $[\text{Mn}(\text{salen})](\text{ClO}_4) \cdot 2\text{H}_2\text{O}$ (106 mg, 0.232 mM) was added at room temperature. The reaction mixture was heated to 60 °C and stirred under argon for 6 h, resulting in a purple solution. NH_4PF_6 (37.8 mg, 0.232 mM) was then added to the above reaction solution. A red precipitate appeared immediately and was collected. Deep red crystals (97.1 mg, 52%) of **1** suitable for X-ray diffraction were obtained by slowly diffusing diethyl-ether into the DMF solution of the red-purple precipitate at room temperature. Anal. Calcd for $\text{FeMnC}_{38}\text{H}_{30}\text{N}_8\text{O}_2\text{PF}_6$: C, 51.49; H, 3.41; N, 12.64%. Found: C, 51.43; H, 3.65; N, 12.64%. IR (KBr pellet, cm^{-1}): 2087 (CN), 2071 (CN). UV-vis (CH_3CN), λ_{max} , nm (ϵ , $\text{dm}^3 \text{M cm}^{-1}$): 382 (10,238), 567 (5557). MS, m/z : 321.6 $[\text{Mn}(\text{salen})]^+$, 443.3 $[\text{Fe}(\text{bpy})_2(\text{CN})_2 + \text{Na}]^+$, 741.0 $[\text{1-PF}_6]^+$.

2.4. Synthesis of $[\text{cis-Ru}(\text{bpy})_2(\text{CN})_2\text{Mn}(\text{salen})][\text{PF}_6]$ (**2**)

The preparation of **2** was similar to that described above for **1**, only $\text{cis-Fe}(\text{bpy})_2(\text{CN})_2 \cdot 3\text{H}_2\text{O}$ (100 mg, 0.211 mM) was replaced by $\text{cis-Ru}(\text{bpy})_2(\text{CN})_2 \cdot 2\text{H}_2\text{O}$ (100 mg, 0.199 mM). Yield yellow crystals (98.5 mg, 53%). Anal. Calcd for $\text{RuMnC}_{38}\text{H}_{30}\text{N}_8\text{O}_2\text{PF}_6$: C, 48.99; H, 3.25; N, 12.03%. Found: C, 48.74; H, 3.69; N, 12.10%. IR (KBr pellet, cm^{-1}): 2085 (CN), 2059 (CN). UV-vis (CH_3CN), λ_{max} , nm (ϵ , $\text{dm}^3 \text{M cm}^{-1}$): 341 (13,837), 412 (8518), 466 (9417). MS, m/z : 321.6 $[\text{Mn}(\text{salen})]^+$, 488.1 $[\text{Ru}(\text{bpy})_2(\text{CN})_2 + \text{Na}]^+$, 787.1 $[\text{2-PF}_6]^+$.

2.5. Synthesis of $[\text{cis-Os}(\text{bpy})_2(\text{CN})_2\text{Mn}(\text{salen})][\text{PF}_6]$ (**3**)

The preparation of **3** was similar to that described above for **1**, only $\text{cis-Fe}(\text{bpy})_2(\text{CN})_2 \cdot 3\text{H}_2\text{O}$ (100 mg, 0.211 mM) was replaced by $\text{cis-Os}(\text{bpy})_2(\text{CN})_2 \cdot 2\text{H}_2\text{O}$ (100 mg, 0.169 mM). Yield brown crystals (77.8 mg, 45%). Anal. Calcd for $\text{OsMnC}_{38}\text{H}_{30}\text{N}_8\text{O}_2\text{PF}_6$: C, 44.71; H, 2.96; N, 10.98%. Found: C, 44.13; H, 3.19; N, 10.96%. IR (KBr pellet, cm^{-1}): 2073 (CN), 2040 (CN). UV-vis (CH_3CN), λ_{max} , nm (ϵ , $\text{dm}^3 \text{M cm}^{-1}$): 326 (15,413), 471 (10,540). MS, m/z : 321.6 $[\text{Mn}(\text{salen})]^+$, 556.3 $[\text{Os}(\text{bpy})_2(\text{CN})_2 + \text{H}]^+$, 875.1 $[\text{3-PF}_6]^+$.

2.6. Synthesis of $[\text{cis-Os}(\text{bpy})_2(\text{CN})_2\text{Mn}(\text{salcy})][\text{PF}_6]$ (**4**)

The preparation of **4** was similar to that described above for **3**, only $[\text{Mn}(\text{salen})(\text{H}_2\text{O})_2](\text{ClO}_4)$ was replaced by $[\text{Mn}(\text{salcy})(\text{H}_2\text{O})_2](\text{ClO}_4)$. Yield black brown crystals (63.7 mg, 35%). Anal.

Calcd for $\text{OsMnC}_{42}\text{H}_{36}\text{N}_8\text{O}_2\text{PF}_6$: C, 46.93; H, 3.38; N, 10.42%. Found: C, 46.30; H, 3.29; N, 10.57%. IR (KBr pellet, cm^{-1}): 2031 (CN), 2062 (CN). UV-vis (CH_3CN), λ_{max} , nm (ϵ , $\text{dm}^3 \text{M cm}^{-1}$): 403 (20,343), 453 (14,953), 511 (13,251), 676(3062). MS, m/z : 375.5 [$\text{Mn}(\text{salcy})$] $^+$, 577.3 [$\text{Os}(\text{bpy})_2(\text{CN})_2 + \text{Na}$] $^+$, 929.3 [$\mathbf{4}\text{-PF}_6$] $^+$.

2.7. Crystallographic data and structure determination

The single-crystal data of **1–4** were collected on Saturn724 + CCD diffractometers equipped with graphite-monochromated Mo- K_α ($\lambda = 0.71073 \text{ \AA}$) radiation using an ω scan mode at 123 K. The structures were solved by direct methods and refined using *SHELXL-97* program suite [17]. Hydrogens were calculated geometrically and refined using a riding model. Anisotropic thermal parameters were used for the non-hydrogen atoms, and isotropic parameters were used for hydrogens. All non-hydrogen atoms were refined by full-matrix least-squares on F^2 . The R values are defined as $R_1 = \Sigma||F_o| - |F_c||/\Sigma|F_o|$ and $\omega R_2 = [\Sigma[\omega(F_o^2 - F_c^2)^2]/\Sigma[\omega(F_o^2)^2]]^{1/2}$. The detailed crystal data for **1–4** are summarized in table 1, and selected bond lengths and angles for **1–4** are presented in table 2.

3. Results and discussion

3.1. Synthesis and characterization

Reaction of Mn(III) Schiff bases with *cis*-dicyanide precursors *cis*- $\text{M}(\text{bpy})_2(\text{CN})_2$ ($\text{M} = \text{Fe}$, Ru, Os), respectively, in the presence of NH_4PF_6 in CH_3OH yielded 1-D heteronuclear zigzag chain complexes [*cis*- $\text{M}(\text{bpy})_2(\text{CN})_2\text{Mn}(\text{salen})$](PF_6) ($\text{M} = \text{Fe}$, **1**; $\text{M} = \text{Ru}$, **2**; $\text{M} = \text{Os}$, **3**) and [*cis*- $\text{Os}(\text{bpy})_2(\text{CN})_2\text{Mn}(\text{salcy})$](PF_6) (**4**). By slow diffusion of Et_2O into the DMF solution of these complexes, brown red to brown black crystals of **1–4** were obtained which were suitable for single-crystal X-ray diffraction analysis. Complexes **1–4** were characterized by IR, MS, elemental analysis, and single-crystal X-ray diffraction analysis. They are all air stable in both the solid state and in solution at ambient temperature.

3.2. Description of the crystal structures of **1–4**

Experimental crystallographic data for **1–4** are given in table 1, and selected bond lengths and angles in table 2. The molecular structures of **1–3** are shown in figure 1, and the molecular structure of **4** is shown in figure 2. Complexes **1–3** crystallized in a monoclinic $C2/c$ space group, while **4** crystallized in the rhombohedral $R\bar{3}$ space group.

In **1–4**, each $\text{M}(\text{bpy})_2(\text{CN})_2$ unit is connected to two [$\text{Mn}^{\text{III}}(\text{salen})$] $^+$ or [$\text{Mn}^{\text{III}}(\text{salcy})$] $^+$ cations via CN groups in *cis*-conformation, and each [$\text{Mn}^{\text{III}}(\text{salen})$] $^+$ or [$\text{Mn}^{\text{III}}(\text{salcy})$] $^+$ cation linked to two $\text{M}(\text{bpy})_2(\text{CN})_2$ in *trans*-conformation, resulting in a zigzag chain structure linked alternately by $\text{M}(\text{bpy})_2(\text{CN})_2$ and [$\text{Mn}^{\text{III}}(\text{salen})$] $^+$ or [$\text{Mn}^{\text{III}}(\text{salcy})$] $^+$. The central M^{II} is octahedral coordinated by four nitrogens from bpy ligands and two carbons from two cyanide groups in a *cis*-configuration.

The bond lengths of $\text{C}\equiv\text{N}$ vary from 1.143(5) to 1.170(5) \AA for **1**, 1.159(8) to 1.160(8) \AA for **3**, and 1.170(13) to 1.174(13) \AA for **4**. The bond distances of $\text{M}(\text{II})\text{-C}(\text{CN})$ increase from 1.892(4) to 1.905(4) \AA for **1**, 1.970(6) to 1.975(6) \AA for **3**, and 1.969(11)–1.974(11) \AA for **4** due to increasing radii from Fe to Os. The bond lengths of Fe-N4 (1.994(3) \AA) and

Table 1. Detail of the crystallographic data collection, structural determination and refinement for 1–4.

	1	2	3	4
Chemical formula	$\text{C}_{38}\text{H}_{30}\text{F}_6\text{MnN}_8\text{O}_2\text{PFe}$	$\text{C}_{38}\text{H}_{30}\text{F}_6\text{MnN}_8\text{O}_2\text{PRu}$	$\text{C}_{38}\text{H}_{30}\text{F}_6\text{MnN}_8\text{O}_2\text{POs}$	$\text{C}_{288}\text{H}_{500}\text{F}_{36}\text{Mn}_6\text{N}_{60}\text{O}_{24}\text{Os}_6\text{P}_6$
Formula weight	886.46	931.68	1020.81	7326.54
Color and habit	Red prism	Red prism	Brown prism	Brown prism
Crystal size, mm	$0.79 \times 0.33 \times 0.10$	$0.30 \times 0.20 \times 0.05$	$0.80 \times 0.60 \times 0.50$	$0.46 \times 0.10 \times 0.07$
T/K	123	123	123	123
Crystal system	Monoclinic	Monoclinic	Monoclinic	Rhombohedral
Space group	$C2/c$	$C2/c$	$C2/c$	$R\bar{3}$
a (Å)	27.177(14)	27.028(17)	27.216(2)	43.655(15)
b (Å)	12.285(5)	12.320(7)	12.320(7)	43.655(15)
c (Å)	24.353(12)	24.701(15)	24.8094(17)	14.930(6)
α (°)	90	90	90	90
β (°)	105.864(9)	106.580(13)	105.996(4)	90
γ (°)	90	90	90	120
V (Å ³)	7821(6)	7883(8)	7998.4(10)	24,642(16)
Z	8	8	8	3
$D_{\text{calcd}}/\text{g cm}^{-3}$	1.506	1.570	1.695	1.481
μ/mm^{-1}	0.809	0.818	3.602	2.648
Completeness	97.5%	99.6%	97.1%	98.4%
$F(0\ 0\ 0)$	3600	3744	4000	10,980
h, k, l range	$-35 \leq h \leq 35, -15 \leq k \leq 15, -31 \leq l \leq 31$	$-32 \leq h \leq 32, -14 \leq k \leq 11, -29 \leq l \leq 29$	$-35 \leq h \leq 35, -10 \leq k \leq 16, -32 \leq l \leq 32$	$-51 \leq h \leq 51, -51 \leq k \leq 51, -17 \leq l \leq 17$
θ Range (°)	2.37–27.49	2.35–25.00	2.64–27.50	2.37–25.00
Reflections measured	8754	6930	8927	9486
Independent reflections	7639	4750	7380	8999
R_{int}	0.0816	0.0501	0.0377	0.1073
GOF	1.079	1.057	1.075	1.169
R_1, wR_2 [$I > 2\sigma(I)$]	0.0822, 0.2379	0.0887, 0.1664	0.0489, 0.1293	0.0885, 0.2226
R_1, wR_2 (all data)	0.0898, 0.2497	0.1222, 0.1850	0.0598, 0.1408	0.0922, 0.2264

Table 2. Selected bond lengths (Å) and angles (°) for 1–4.

	1	2	3	4
M1–C1	1.905(4)	1.972(11)	1.975(6)	1.974(11)
M1–C2	1.892(4)	1.957(10)	1.970(6)	1.969(11)
M1–N3	1.974(4)	2.045(9)	2.065(6)	2.065(8)
M1–N4	1.994(3)	2.098(8)	2.107(5)	2.102(9)
M1–N5	2.002(3)	2.089(8)	2.117(5)	2.098(8)
M1–N6	1.967(4)	2.043(9)	2.069(6)	2.073(9)
Mn1–N1	2.261(3)	2.254(9)	2.245(5)	2.285(8)
Mn1–N2	2.254(3)	2.254(9)	2.232(6)	2.209(9)
C1–N1	1.143(5)	1.150(11)	1.159(8)	1.170(13)
C2–N2	1.170(5)	1.147(11)	1.160(8)	1.174(13)
C1–M1–C2	87.36(14)	87.4(4)	88.0(2)	91.7(4)
N1–C1–M1	176.1(3)	177.1(8)	176.9(5)	177.5(10)
N2–C2–M2	179.9(5)	178.6(10)	178.0(7)	177.8(7)
C1–N1–Mn1	158.1(3)	146.2(8)	145.7(5)	144.9(8)
C2–N2–Mn2	148.7(3)	158.7(8)	159.3(6)	159.4(9)
O1–Mn1–O2	94.97(11)	94.1(3)	94.26(19)	93.9(3)
N1–Mn1–N2	170.59(12)	172.1(3)	172.1(2)	172.2(3)
M1···Mn1	5.1	5.1	5.1	5.2
M1···Mn2	5.2	5.3	5.3	5.3
Mn1···Mn2	6.6	6.6	6.8	7.3

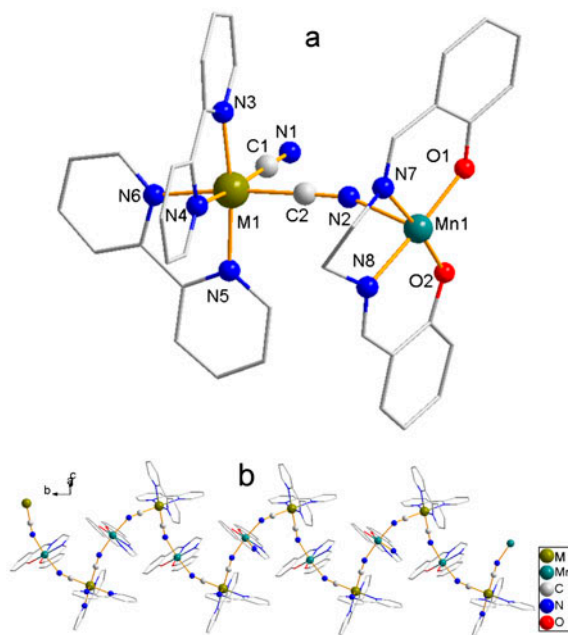


Figure 1. (a) Crystal structures of heteronuclear complexes $[cis\text{-}M(\text{bpy})_2(\text{CN})_2\text{Mn}(\text{salen})][\text{PF}_6]$ ($M = \text{Fe}$, **1**; $M = \text{Ru}$, **2**; $M = \text{Os}$, **3**); (b) side perspective drawing of 1-D chain complexes **1–3**. Hydrogens and PF_6^- have been omitted for clarity.

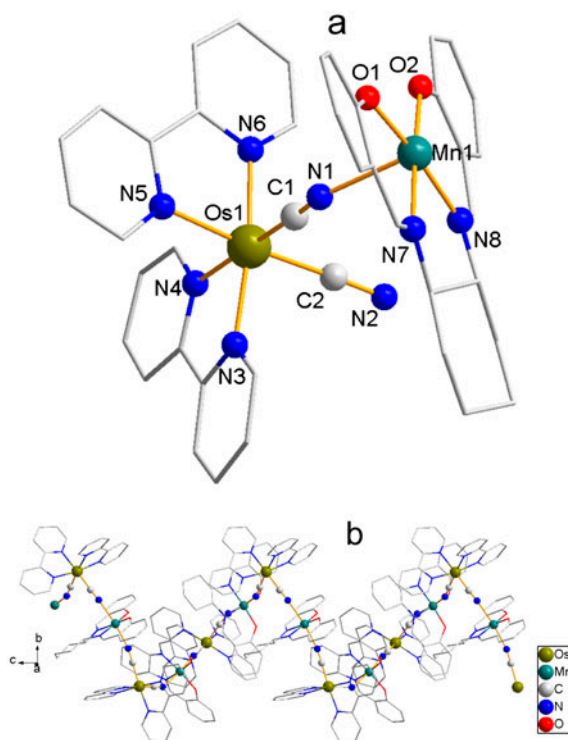


Figure 2. (a) Crystal structures of heteronuclear complex **4**; (b) side perspective drawing of 1-D chain complex **4**. Hydrogens, PF_6^- , and solvent molecules have been omitted for clarity.

Fe–N5 (2.002(3) Å) are longer than that of Fe–N3 (1.974(4) Å) and Fe–N6 (1.967(4) Å) in **1** owing to the structural *trans*-effect [18]. Similar phenomena can also be found in **2–4** from table 2.

In the distorted octahedral coordination geometry around Mn^{III} , the equatorial sites are occupied by the N_2O_2 donors from the tetradentate salen Schiff base ligand, and the axial positions are occupied by two nitrogens from the bridging CN^- groups in a *trans*-position with $\text{Mn}(\text{III})\text{-N}(\text{CN})$ distances of 2.254(3) Å and 2.261(3) Å for **1**. Different from the near linearity of $\text{Fe}(\text{II})\text{-C}\equiv\text{N}$ with $176.1(3)^\circ$ and $179.9(5)^\circ$, the $\text{Mn}(\text{III})\text{-N}\equiv\text{C}(\text{CN})$ bond angles are $158.1(3)^\circ$ and $148.7(3)^\circ$ in **1**. Similar behavior can also be found in **2–4**.

Similar to other $\text{Mn}(\text{salen})$ -based complexes [19], the packing of bimetallic chains is often dominated by aromatic $\pi\text{-}\pi$ stacking interactions. For **1–4**, the chains run along the *b* direction and form layers parallel to the *bc* plane. The shortest distances between two neighboring chains are 4.10 Å (**1**), 4.00 Å (**2**), 3.95 Å (**3**), and 4.64 Å (**4**) (figures S1–S4, see online supplemental material at <http://dx.doi.org/10.1080/00958972.2014.981537>), which are longer than the $\pi\text{-}\pi$ stacking distance of 3.4–3.6 Å [20], suggesting the interactions between adjacent chains can be neglected in **1–4**. The neighboring $\text{M}^{\text{II}}\cdots\text{Mn}^{\text{III}}$ distances are 5.1 and 5.2 Å for **1**, 5.1 and 5.3 Å for **2**, 5.1 and 5.3 Å for **3**, and 5.2 and 5.3 Å for **4**. The shortest intrachain $\text{Mn}^{\text{III}}\cdots\text{Mn}^{\text{III}}$ separations are 6.6 Å for **1–3** and 7.3 Å for **4**. The nearest interchain $\text{Mn}^{\text{III}}\cdots\text{Mn}^{\text{III}}$ distances are 11.4, 11.6, 11.7, and 10.6 Å for **1–4**, respectively, indicating the interchain $\text{Mn}^{\text{III}}\text{-Mn}^{\text{III}}$ interactions can be neglected.

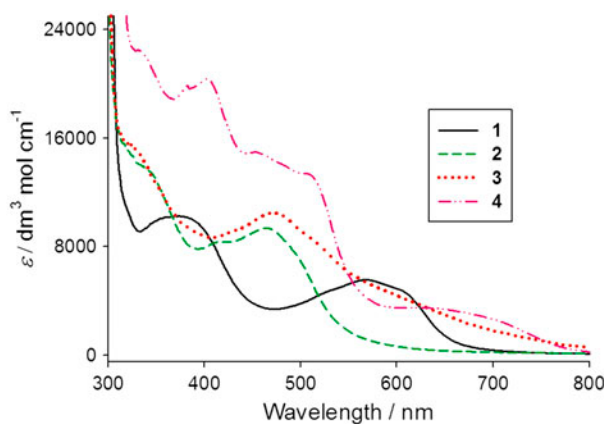
Table 3. Data of cyclic voltammetry, cyanide stretching frequencies, and electronic absorption spectra.

Compound	P/V	ν_{CN} (cm^{-1})	λ_{max} , nm (ϵ , $\text{dm}^3 \text{M}^{-1} \text{cm}^{-1}$)
<i>cis</i> -Fe(bpy) ₂ (CN) ₂ ·3H ₂ O	0.46 ^a	2069, 2079 ^a	382 (6200), 590 (6280)
<i>cis</i> -Ru(bpy) ₂ (CN) ₂ ·2H ₂ O	0.86 ^b	2053, 2067 ^b	346 (9428), 483 (10,385)
<i>cis</i> -Os(bpy) ₂ (CN) ₂ ·2H ₂ O	0.47	2040, 2057	348 (11,791), 382 (11,543), 458 (10,665), 506 (13,000), 650 (3370)
[Mn(salen)(H ₂ O) ₂](ClO ₄)	—	—	402 (5948)
[Mn(salcy)(H ₂ O) ₂](ClO ₄)	—	—	406 (3944)
1	-0.39 ^c , 0.38	2071, 2087	382 (10,238), 567 (5557)
2	-0.38 ^c , 0.76	2059, 2085	341 (13,837), 412(8518), 466 (9417)
3	-0.36 ^c , 0.37	2040, 2073	326 (15,413), 471 (10,540)
4	-0.13, 0.35	2031, 2062	403 (20,343), 453 (14,953), 511(13,251), 676 (3062)

^aRef. [37].^bRef. [38].^cIrreversible wave.

3.3. IR spectroscopy

The cyanide stretching frequencies for **1–4** and related precursor mononuclear compounds are listed in table 3. For cyanide-bridged complexes, the ν_{CN} stretching vibrations are typical. There are two ν_{CN} bands for **1–4**, which are the symmetric and asymmetric stretches in the *cis*-complexes. The ν_{CN} of the cyanide-bridged complexes (**1–4**) are higher than that of their precursors, attributed to both kinematical coupling occurring when a second metal is attached to the CN and to the fact that the cyanide N donated electron density from an anti-bonding molecular orbital to the Mn(III) center, thereby increasing the CN force constant [21]. By comparison of the ν_{CN} of **1–4**, two rules can be found: (i) the heavier the metal, the lower frequency of the two ν_{CN} bands; (ii) the separation between the two ν_{CN} bands increases in the order of Fe < Ru < Os. These results are consistent with the detailed study of mononuclear complexes [22]. The lower ν_{CN} stretching vibrations of **4** than that of **3** can be attributed to the effect of different ligand (salen *versus* salcy). The strong peak at 841 cm^{-1} for **1–4** can be attributed to the stretching vibration of PF_6^- .

Figure 3. Electronic absorption spectrum of **1–4** in CH₃CN.

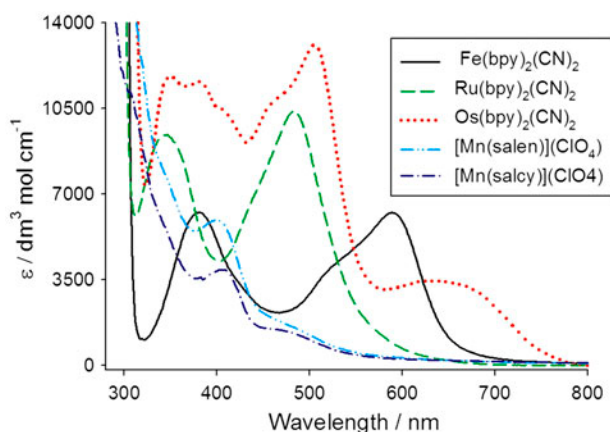


Figure 4. Electronic absorption spectra of precursors in CH_3CN .

3.4. Electronic absorption spectroscopy

Electronic absorption spectra of **1–4** and their precursors were measured in CH_3CN solution at room temperature. The electronic absorption spectra of **1–4** are presented in figure 4, and the detailed data of **1–4** are listed in table 3. For comparison, the electronic absorption spectra and the data of the related precursors $\text{Fe}(\text{bpy})_2(\text{CN})_2 \cdot 3\text{H}_2\text{O}$ [12a, 14, 23], *cis*-Ru($\text{bpy})_2(\text{CN})_2 \cdot 2\text{H}_2\text{O}$ [14] and *cis*-Os($\text{bpy})_2(\text{CN})_2 \cdot 2\text{H}_2\text{O}$ [14] are also shown in figure 3 and listed in table 3. By comparison with the precursors, the maximum absorption wavelength at 567 nm for **1**, 466 nm for **2**, and 471 nm for **3** can be ascribed to $M^{\text{II}} \rightarrow \text{bpy}$ ($M = \text{Fe, Ru}$ and Os) metal to ligand charge transfer (MLCT). The maximum absorption band ($\text{Fe}^{\text{II}} \rightarrow \text{bpy}$ MLCT) is blue-shifted from the precursor *cis*- $\text{Fe}(\text{bpy})_2(\text{CN})_2$ (590 nm) to **1** (567 nm). This shift can be interpreted as an increase in $d\pi(\text{Fe}) \rightarrow \pi^*(\text{bpy})$ back bonding and a concomitant decrease in $\sigma(\text{Fe}) \rightarrow \sigma(\text{bpy})$ bonding upon forming $\text{Fe}\text{--}\text{CN}\text{--}\text{Mn}$ [24]. Such blue-shifted behavior could also be observed in **2** and **3**. The maximum absorption wavelength of **1–3** increases in the order $\text{Ru} < \text{Os} < \text{Fe}$. Similar phenomenon has also been reported [14b, 25]. This might result from the nature of the heavier Os, such as the more diffuse nature of the 5d orbital with respect to 4d and 3d orbitals [26] and larger spin-orbit coupling of Os than Ru and Fe [27]. The electronic absorption of **4** is more complicated, and the reason is unclear [14b].

3.5. Electrochemistry

Cyclic voltammetry studies were carried out on **1–4** to determine their redox properties, as well as to establish whether the related complexes were stable and potentially isolable. All four complexes were subjected to cyclic voltammetry in acetonitrile solution. The electrochemical data for **1–4** in acetonitrile are listed in table 3, and the cyclic voltammograms of **1–4** are shown in figures 5–8.

The cyclic voltammograms of **1–3** in acetonitrile showed reversible ($\Delta E_p = 60\text{--}80$ mV) redox processes at +0.38 V, +0.76 V, and +0.37 V, and an irreversible reductive couple at -0.39 V, -0.38 V, and -0.36 V, respectively (figures 5–7). Complex **4** displays two reversible redox processes at 0.35 V ($\Delta E_p = 80$ mV) and -0.13 V ($\Delta E_p = 60$ mV). The first waves in cyclic voltammograms of **1–4** are assigned to the $M^{\text{II/III}}(\text{bpy})_2(\text{CN})_2$ processes ($M = \text{Fe,}$

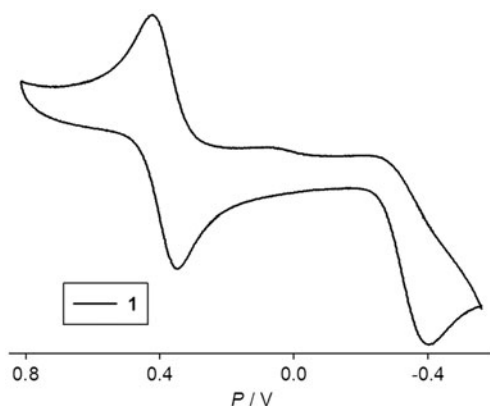


Figure 5. Cyclic voltammogram of **1** in CH₃CN containing 0.1 M (Bu₄N)(PF₆) electrolyte. Scan rate was 100 mV s⁻¹.

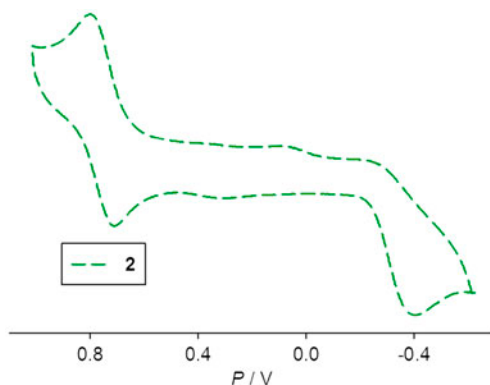


Figure 6. Cyclic voltammogram of **2** in CH₃CN containing 0.1 M (Bu₄N)(PF₆) electrolyte. Scan rate was 100 mV s⁻¹.

Ru and Os). Their potentials are close to those of related mononuclear precursors *cis*-M(bpy)₂(CN)₂. The second reductive/redox waves are assigned to the Mn(salen) or Mn(salicy)-cores, representing the Mn^{III}/Mn^{II} process. Also, the potentials are close to other mononuclear Mn(III) Schiff bases [28]. The abnormal trend that the reversible redox wave of the Os-based complexes (0.37 V in **3** and 0.35 V in **4**) is lower than that of the Ru-based complex (0.76 V in **2**) is consistent with the related precursors *cis*-M^{II}(bpy)₂(CN)₂, the reason might be ascribed to the larger spin-orbit coupling of Os(II) than Ru(II) [27].

3.6. Magnetic properties

The variable-temperature magnetic susceptibilities of **1** were measured under an external magnetic field of 1000 Oe at 2–300 K using a SQUID magnetometer. As shown in figure 9, the $\chi_M T$ value of **1** is 3.10 cm³ K M⁻¹ at 300 K, in good agreement with the spin-only value of 3.00 cm³ K M⁻¹ expected for a diamagnetic low-spin (LS) Fe(II) ion and a high-spin (HS) Mn(III) ion system ($S_{\text{Fe(II)}}=0$, $S_{\text{Mn(III)}}=2$) with $g = 2.0$. On lowering the temperature, the $\chi_M T$ value of **1** is almost constant until 20 K, then gradually changes to 2.94 cm³

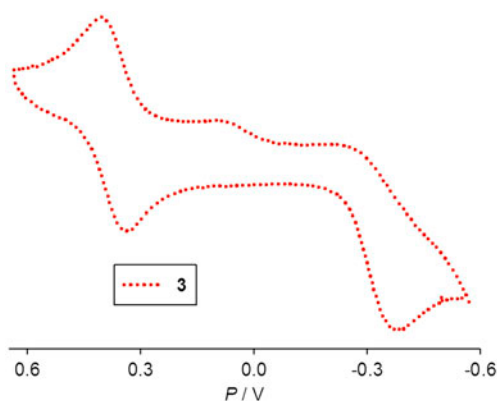


Figure 7. Cyclic voltammogram of **3** in CH_3CN containing 0.1 M $(\text{Bu}_4\text{N})(\text{PF}_6)$ electrolyte. Scan rate was 100 mV s^{-1} .

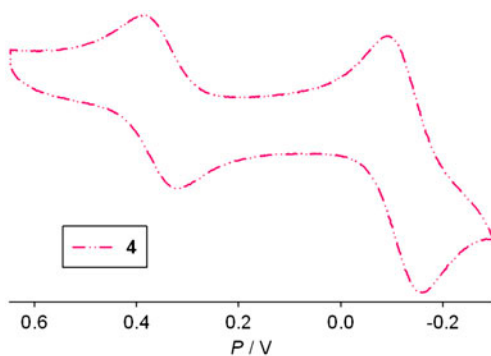


Figure 8. Cyclic voltammogram of **4** in CH_3CN containing 0.1 M $(\text{Bu}_4\text{N})(\text{PF}_6)$ electrolyte. Scan rate was 100 mV s^{-1} .

K M^{-1} at 10 K, finally sharply decreasing with further decreasing temperature to $2.53 \text{ cm}^3 \text{ K M}^{-1}$ at 2.0 K. The rapid decrease of $\chi_{\text{M}}T$ at low temperature might be attributed to the zero-field splitting (ZFS) effect or the magnetic interaction through space [29]. The magnetic susceptibilities of **1** obey the Curie–Weiss law and could be fitted based on $\chi_{\text{M}} = C/(T-\theta)$, affording $C = 3.066 \text{ cm}^3 \text{ K M}^{-1}$ and $\theta = -0.50 \text{ K}$. When considering the regular chain of **1** as 1-D Heisenberg model with Hamiltonian $\mathbf{H} = -2J \sum \mathbf{S}_1 \mathbf{S}_2$ [30], the following empirical equation could be used to fit the magnetic data for **1**: $\chi_{\text{M}} = Ng^2\beta^2/(kT) \times (A + Bx^2)/(1 + Cx + Dx^3)$, with $x = |J|/kT$. For HS Mn(III), $S = 2.0$ with $A = 2.000$, $B = 71.938$, $C = 10.48$, $D = 955.56$ [31], where N , g , k , β , and J are Avogadro's number, g -factor, the Boltzmann constant, the Bohr magneton, and exchange coupling parameter, respectively. Using the above 1-D model for **1** from 2 to 300 K, the best-fitting leads to $J = -0.038 \text{ cm}^{-1}$, $g = 2.03$, and $R = \Sigma(\chi_{\text{calcd}}T - \chi_{\text{obsd}}T)^2 / \Sigma(\chi_{\text{obsd}}T)^2 = 4.9 \times 10^{-4}$. The value of exchange coupling constant (J) is close to other paramagnetic centers linked by diamagnetic $\text{--NC--Fe(II)--CN--}$ bridges [32]. In general, the effect of Mn(III) anisotropy should be taken into account for the study of magnetic properties of Mn(salen) complexes [33]. However, attempts to simulate the experimental data for **1** using the magnetic model considering the Mn(III) anisotropy [34] did not lead to an acceptable fit. This suggests that, similar to

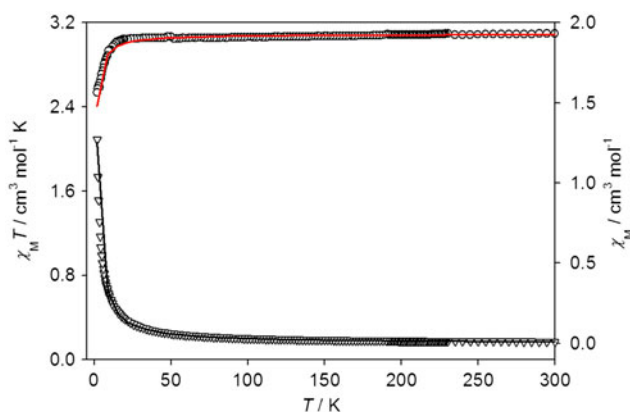


Figure 9. Magnetic behavior of **1** as measured in an applied field of 1000 Oe using a SQUID magnetometer. Fitting (black line) on χ_M vs. T (triangle) and fitting (red line) on $\chi_M T$ vs. T (circle) of **1** in the crystalline samples (see <http://dx.doi.org/10.1080/00958972.2014.981537> for color version).

some previous reports [33c, 33d], the effect of the Mn(III) anisotropy could be neglected for **1**.

The temperature dependent magnetic susceptibilities for **2–4** were collected at 1000 Oe from 2–300 K using a SQUID magnetometer (figures 10–12). Similar to **1**, the $\chi_M T$ values for **2** ($3.00 \text{ cm}^3 \text{ K M}^{-1}$), **3** ($2.96 \text{ cm}^3 \text{ K M}^{-1}$), and **4** ($2.93 \text{ cm}^3 \text{ K M}^{-1}$) at 300 K are close to the expected theoretical value of $3.00 \text{ cm}^3 \text{ K M}^{-1}$. Upon cooling, the $\chi_M T$ values of **2–4** slightly increase linearly until $3.06 \text{ cm}^3 \text{ K M}^{-1}$ for **2**, $3.06 \text{ cm}^3 \text{ K M}^{-1}$ for **3**, and $3.11 \text{ cm}^3 \text{ K M}^{-1}$ for **4** at 38 K, finally sharply decreasing with further decreasing temperature to $2.96 \text{ cm}^3 \text{ K M}^{-1}$ for **2**, $2.21 \text{ cm}^3 \text{ K M}^{-1}$ for **3**, and $2.25 \text{ cm}^3 \text{ K M}^{-1}$ for **4** at 2.0 K. Similar to **1**, the sharp decrease of $\chi_M T$ values of **2–4** at low temperature are attributed to zero-field splitting (ZFS) effect or the magnetic interaction through space [29]. The linear increase in $\chi_M T$ with decreasing temperature from 300 to 48 K for **2–4** should result from spin-orbit coupling in Mn(III) ion (typical contribution of a temperature-independent paramagnetism,

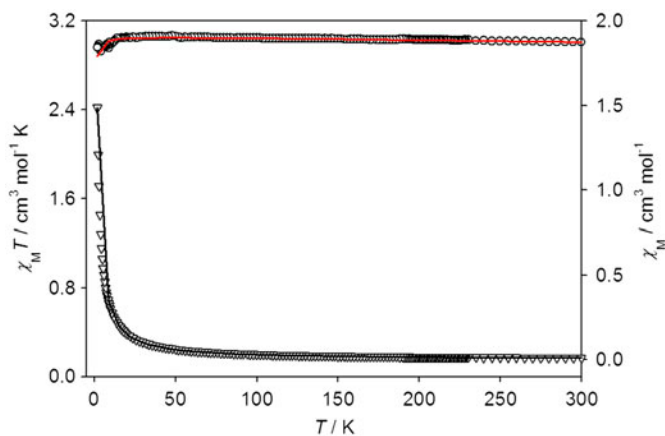


Figure 10. Magnetic behavior of **2** as measured in an applied field of 1000 Oe using a SQUID magnetometer. Fitting (black line) on χ_M vs. T (triangle) and fitting (red line) on $\chi_M T$ vs. T (circle) of **2** in the crystalline samples (see <http://dx.doi.org/10.1080/00958972.2014.981537> for color version).

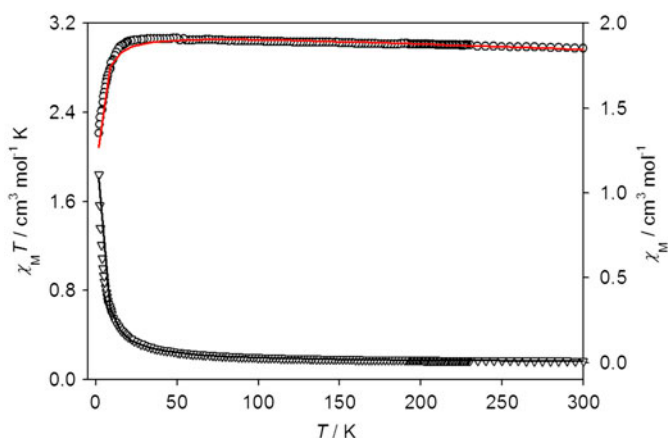


Figure 11. Magnetic behavior of **3** as measured in an applied field of 1000 Oe using a SQUID magnetometer. Fitting (black line) on χ_M vs. T (triangle) and fitting (red line) on $\chi_M T$ vs. T (circle) of **3** in the crystalline samples (see <http://dx.doi.org/10.1080/00958972.2014.981537> for color version).

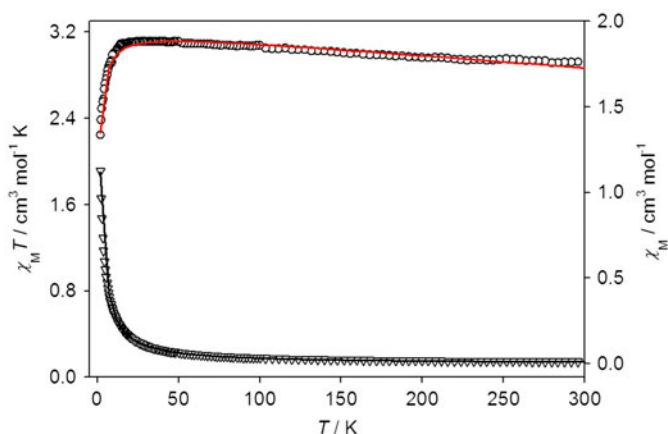


Figure 12. Magnetic behavior of **4** as measured in an applied field of 1000 Oe using a SQUID magnetometer. Fitting (black line) on χ_M vs. T (star) and fitting (red line) on $\chi_M T$ vs. T (circle) of **4** in the crystalline samples (see <http://dx.doi.org/10.1080/00958972.2014.981537> for color version).

χ_{TIP} [35] due to the effect of the heavy Ru(II) and Os(II). Thereby, a TIP ($N\alpha$) should be added to the magnetic data fitting for **2–4**, so the equation for fitting the exchange coupling of **2–4** should be described as $\chi_M = Ng^2\beta^2/(kT) \times (A + Bx^2)/(1 + Cx + Dx^3) + N\alpha$. The obtained best-fit parameters are $J = -0.0085 \text{ cm}^{-1}$, $g = 2.02$, $N\alpha = -1.8 \times 10^{-4} \text{ cm}^3 \text{ M}^{-1}$, and $R = 2.0 \times 10^{-4}$ for **2**; $J = -0.069 \text{ cm}^{-1}$, $g = 2.05$, $N\alpha = -6.0 \times 10^{-4} \text{ cm}^3 \text{ M}^{-1}$, and $R = 6.0 \times 10^{-4}$ for **3**; and $J = -0.059 \text{ cm}^{-1}$, $g = 2.07$, $N\alpha = -1.2 \times 10^{-4} \text{ cm}^3 \text{ M}^{-1}$, and $R = 6.9 \times 10^{-4}$ for **4**. The values of exchange constant are close to that of paramagnetic Mn(III) ions linked by diamagnetic -NC-M(II)-CN- bridges [36]. To evaluate the Curie–Weiss constants of **2–4**, a TIP ($N\alpha$) should also be added to the Curie–Weiss law. Using the equation $\chi_M = C/(T - \theta) + N\alpha$, the parameters are obtained as follows: $C = 2.976 \text{ cm}^3 \text{ K M}^{-1}$, $\theta = -0.012 \text{ K}$, and $N\alpha = 7 \times 10^{-4} \text{ cm}^3 \text{ M}^{-1}$ for **2**; $C = 2.980 \text{ cm}^3 \text{ K M}^{-1}$, $\theta = -0.750 \text{ K}$, and $N\alpha = 1.07 \times 10^{-3} \text{ cm}^3 \text{ M}^{-1}$ for **3**; and $C = 3.240 \text{ cm}^3 \text{ K M}^{-1}$, $\theta = -0.890 \text{ K}$, and $N\alpha$

$= -1.08 \times 10^{-3} \text{ cm}^3 \text{ M}^{-1}$ for **4**. Similar to **1**, attempts to simulate the experimental data for **2–4** using the magnetic model considering the Mn(III) anisotropy [34] did not lead to an acceptable fit. Thus, the effect of the Mn(III) anisotropy [33c, 33d] can be neglected for **2–4**. By comparison with the magnetic properties of the complexes reported [11a, 11b], the magnetic behaviors of **1–4** indicate that the magnetic coupling between paramagnetic metal ions across the diamagnetic cyanidometal bridge is very weak and can be neglected.

4. Conclusion

Four new cyanido-bridged 1-D heteronuclear zigzag chain complexes, $[\text{cis-M}(\text{bpy})_2(\text{CN})_2\text{Mn}(\text{salen})(\text{PF}_6)]$ ($\text{M} = \text{Fe}$, **1**; $\text{M} = \text{Ru}$, **2**; $\text{M} = \text{Os}$, **3**) and $[\text{cis-Os}(\text{bpy})_2(\text{CN})_2\text{Mn}(\text{salcyl})](\text{PF}_6)$ (**4**) have been synthesized and fully characterized. IR spectra of **1–4** suggest that ν_{CN} increases in the series of $\text{Os} < \text{Ru} < \text{Fe}$ and the separation between the two ν_{CN} bands increases in the order of $\text{Fe} < \text{Ru} < \text{Os}$. The maximum absorption wavelength ($\text{M}^{\text{II}} \rightarrow \text{bpy}$ MLCT) of **1–3** is blue-shifted with respect to their precursors $\text{cis-M}(\text{bpy})_2(\text{CN})_2$ and increases in the order of $\text{Ru} < \text{Os} < \text{Fe}$. Electrochemical studies indicate for **1–4**, the metal centers and the ligand around the metal ions have significant influence on the reversibility of electrochemistry. Furthermore, this work suggests that the magnetic interactions of the complexes with the diamagnetic cyanidometal bridge are very weak when the paramagnetic cyanide N-bonding metal units are high-spin paramagnetic Mn(III) Schiff bases.

Supplementary material

CCDC-982923 (**1**), CCDC-982924 (**2**), CCDC-982925 (**3**), and CCDC-1010140 (**4**) contain the supplementary crystallographic data, related bond lengths and angles for this article. These data can be obtained free of charge from the Cambridge Crystallographic Data Center via www.ccdc.cam.ac.uk/data_request/cif.

Acknowledgements

We thank 973 Program (2012CB821702 and 2014CB845603), the National Science Foundation of China (21173223 and 21233009) for financial support.

References

- [1] (a) W.R. Entley, G.S. Girolami. *Science*, **268**, 397 (1995); (b) S. Ferlay, T. Mallah, R. Ouahes, P. Veillet, M. Verdaguer. *Nature*, **378**, 701 (1995); (c) M. Verdaguer, A. Bleuzen, V. Marvaud, J. Vaissermann, M. Seuleiman, C. Desplanches, A. Scullier, C. Train, R. Garde, G. Gelly, C. Lomenech, I. Rosenman, P. Veillet, C. Cartier, F. Villain. *Coord. Chem. Rev.*, **192**, 1023 (1999).
- [2] (a) T. Glaser, M. Heidemeier, T. Weyhermüller, R.D. Hoffmann, H. Rupp, P. Müller. *Angew. Chem. Int. Ed.*, **45**, 6033 (2006); (b) D.E. Freedman, D.M. Jenkins, A.T. Iavarone, J.R. Long. *J. Am. Chem. Soc.*, **130**, 2884 (2008); (c) A.V. Pali, S.M. Ostrovsky, S.I. Klokishner, B.S. Tsukerblat, C.P. Berlinguette, K.R. Dunbar, J.R. Galan-Mascaros. *J. Am. Chem. Soc.*, **126**, 16860 (2004); (d) Y. Song, P. Zhang, X. Ren, X. Shen, Y. Li, X. You. *J. Am. Chem. Soc.*, **127**, 3708 (2005).
- [3] (a) M.X. Yao, Q. Zheng, K. Qian, Y. Song, S. Gao, J.L. Zuo. *Chem. Eur. J.*, **19**, 294 (2013); (b) L.M. Toma, J. Pasan, C. Ruiz-Perez, F. Lloret, M. Julve. *Dalton Trans.*, **41**, 13716 (2012); (c) T.D. Harris, M.V. Bennett, R. Clerac, J.R. Long. *J. Am. Chem. Soc.*, **132**, 3980 (2010).

- [4] (a) S. Bonnet, M.A. Siegler, J.S. Costa, G. Molnár, A. Bousseksou, A.L. Spek, P. Gamez, J. Reedijk. *Chem. Commun.*, 5619 (2008); (b) J.H. Yoon, D.W. Ryu, S.Y. Choi, H.C. Kim, E.K. Koh, J. Tao, C.S. Hong. *Chem. Commun.*, **47**, 10416 (2011); (c) I. Boldog, F.J. Muñoz-Lara, A.B. Gaspar, M.C. Muñoz, M. Sereudyk, J.A. Real. *Inorg. Chem.*, **48**, 3710 (2009).
- [5] (a) G. Fornasieri, A. Bleuzen. *Angew. Chem. Int. Ed.*, **47**, 7750 (2008); (b) J.M. Herrera, V. Marvaud, M. Verdaguer, J. Marrot, M. Kalisz, C. Mathoniere. *Angew. Chem. Int. Ed.*, **43**, 5468 (2004); (c) J.D. Cafun, G. Champion, M.A. Arrio, C.C.D. Moulin, A. Bleuzen. *J. Am. Chem. Soc.*, **132**, 11552 (2010); (d) T. Hozumi, K. Hashimoto, S. Ohkoshi. *J. Am. Chem. Soc.*, **127**, 3864 (2005); (e) T. Liu, D.P. Dong, S. Kanegawa, S. Kang, O. Sato, Y. Shiota, K. Yoshizawa, S. Hayami, S. Wu, C. He, C.Y. Duan. *Angew. Chem. Int. Ed.*, **51**, 4367 (2012).
- [6] (a) L.M.C. Beltran, J.R. Long. *Acc. Chem. Res.*, **38**, 325 (2005); (b) Y.H. Li, W.R. He, X.H. Ding, S. Wang, L.F. Cui, W. Huang. *Coord. Chem. Rev.*, **256**, 2795 (2012); (c) L.M. Toma, L.D. Toma, F.S. Delgado, C. Ruiz-Perez, J. Sletten, J. Cano, J.M. Clemente-Juan, F. Lloret, M. Julve. *Coord. Chem. Rev.*, **250**, 2176 (2006); (d) D.P. Zhang, H.L. Wang, Y.T. Chen, Z.H. Ni, L.J. Tian, J.Z. Jiang. *Inorg. Chem.*, **48**, 11215 (2009); (e) H.Z. Kou, S. Gao, B.Q. Ma, D.Z. Liao. *Chem. Commun.*, **713**, (2000); (f) J. Xiang, W.L. Man, J. Guo, S.M. Yiu, G.H. Lee, S.M. Peng, G. Xu, S. Gao, T.C. Lau. *Chem. Commun.*, **46**, 6102 (2010); (g) Y.Z. Zhang, B.W. Wang, O. Sato, S. Gao. *Chem. Commun.*, **46**, 6959 (2010); (h) H. Tokoro, S. Ohkoshi, T. Matsuda, T. Hozumi, K. Hashimoto. *Chem. Phys. Lett.*, **388**, 379 (2004); (i) X.Y. Wang, M.G. Hilfiger, A. Prosvirin, K.R. Dunbar. *Chem. Commun.*, **46**, 4484 (2010); (j) N. Motokawa, S. Matsunaga, S. Takaishi, H. Miyasaka, M. Yamashita, K.R. Dunbar. *J. Am. Chem. Soc.*, **132**, 11943 (2010).
- [7] (a) G. Rogez, A. Marvilliers, E. Rivière, J.P. Audière, F. Lloret, F. Varret, A. Goujon, N. Mendenez, J.J. Girerd, T. Mallah. *Angew. Chem. Int. Ed.*, **39**, 2885 (2000); (b) M. Ohba, H. Okawa. *Coord. Chem. Rev.*, **198**, 313 (2000); (c) H.Z. Kou, S.F. Si, S. Gao, D.Z. Liao, Z.H. Jiang, S.P. Yan, Y.G. Fan, G.L. Wang. *Eur. J. Inorg. Chem.*, **699**, (2002); (d) Z. Smekal, Z. Travnicek, J. Mrozinski, J. Marek. *Inorg. Chem. Commun.*, **6**, 1395 (2003); (e) K. Halbauer, E.T. Spielberg, A. Sterzik, W. Plass, W. Imhof. *Inorg. Chim. Acta*, **363**, 1013 (2010); (f) M. Shatruk, A. Dragulescu-Andrasi, K.E. Chambers, S.A. Stoian, E.L. Bominaar, C. Achim, K.R. Dunbar. *J. Am. Chem. Soc.*, **129**, 6104 (2007); (g) A. Panja, N. Shaikh, P. Vojtisek, S. Gao, P. Banerjee. *New J. Chem.*, **26**, 1025 (2002); (h) A.H. Yuan, L.D. Lu, X.P. Shen, L.Z. Chen, K.B. Yu. *Transit. Met. Chem.*, **28**, 163 (2003); (i) K. Halbauer, G. Leibelng, W. Imhof. *Z. Anorg. Allg. Chem.*, **632**, 264 (2006).
- [8] H.H. Ko, J.H. Lim, H.S. Yoo, J.S. Kang, H.C. Kim, E.K. Koh, C.S. Hong. *Dalton Trans.*, **36**, 2070 (2007).
- [9] Y. Xu, X. Shen, H. Zhou, H. Shu, W. Li, A. Yuan. *J. Mol. Struct.*, **921**, 341 (2009).
- [10] H.Y. Kwak, D.W. Ryu, J.W. Lee, J.H. Yoon, H.C. Kim, E.K. Koh, J. Krinsky, C.S. Hong. *Inorg. Chem.*, **49**, 4632 (2010).
- [11] (a) X. Ma, S.M. Hu, C.H. Tan, Y.H. Wen, Q.L. Zhu, C.J. Shen, T.L. Sheng, X.T. Wu. *Dalton Trans.*, **41**, 12163 (2012); (b) X. Ma, S.M. Hu, C.H. Tan, Y.F. Zhang, X.D. Zhang, T.L. Sheng, X.T. Wu. *Inorg. Chem.*, **52**, 11343 (2013); (c) X. Ma, C.S. Lin, S.M. Hu, C.H. Tan, Y.H. Wen, T.L. Sheng, X.T. Wu. *Chem. Eur. J.*, **20**, 7025 (2014).
- [12] (a) A.A. Schilt. *J. Am. Chem. Soc.*, **82**, 3000 (1960); (b) A.A. Schilt, P.A. Russo, A. Wold. *Inorg. Synth.*, **12**, 247 (1970).
- [13] J.N. Demas, T.F. Turner, G.A. Crosby. *Inorg. Chem.*, **8**, 674 (1969).
- [14] (a) A.A. Schilt. *J. Am. Chem. Soc.*, **85**, 904 (1963); (b) G. Bryant, J. Fergusson, H. Powell. *Aust. J. Chem.*, **24**, 257 (1971).
- [15] (a) Z.H. Ni, L. Zheng, L.F. Zhang, A.L. Cui, W.W. Ni, C.C. Zhao, H.Z. Kou. *Eur. J. Inorg. Chem.*, **1240**, (2007); (b) P. Przychodzen, K. Lewinski, M. Balanda, R. Pelka, M. Rams, T. Wasiutynski, C. Guyard-Duhayon, B. Sieklucka. *Inorg. Chem.*, **43**, 2967 (2004); (c) H. Shyu, H. Wei, Y. Wang. *Inorg. Chim. Acta*, **290**, 8 (1999); (d) H. Li, Z.J. Zhong, C. Duan, X. You, T.C.W. Mak, B. Wu, *J. Coord. Chem.*, **41**, 183 (1997).
- [16] (a) M.X. Yao, Q. Zheng, X.M. Cai, Y.Z. Li, Y. Song, J.L. Zuo. *Inorg. Chem.*, **51**, 2140 (2012); (b) S.R. Korpouju, N. Mangayarkarasi, S. Ameerunisha, E.J. Valente, P.S. Zacharias. *J. Chem. Soc., Dalton Trans.*, (2000).
- [17] (a) G.M. Sheldrick. *Acta Crystallogr. Sect. A.*, **64**, 112 (2008); (b) G.M. Sheldrick. In *Program for X-ray Crystal Structure Refinement*, University of Göttingen, Germany (1997).
- [18] K.M. Anderson, A.G. Orpen. *Chem. Commun.*, **37**, 2682 (2001).
- [19] F. Pan, Z.M. Wang, S. Gao. *Inorg. Chem.*, **46**, 10221 (2007).
- [20] (a) C.A. Hunter, J.K.M. Sanders. *J. Am. Chem. Soc.*, **112**, 5525 (1990); (b) M.L. Głowka, D. Martynowski, K. Kozłowska. *J. Mol. Struct.*, **474**, 81 (1999).
- [21] (a) C.A. Bignozzi, R. Argazzi, J.R. Schoonover, K.C. Gordon, R.B. Dyer, F. Scandola. *Inorg. Chem.*, **31**, 5260 (1992); (b) B.J. Coe, T.J. Meyer, P.S. White. *Inorg. Chem.*, **34**, 3600 (1995).
- [22] A.A. Schilt. *Inorg. Chem.*, **3**, 1323 (1964).
- [23] A.A. Schilt. *J. Am. Chem. Soc.*, **82**, 5779 (1960).
- [24] (a) D.F. Shriver, J. Posner. *J. Am. Chem. Soc.*, **88**, 1672 (1966); (b) N.K. Hamer, L.E. Orgel. *Nature*, **190**, 439 (1961).
- [25] E.M. Kober, T.J. Meyer. *Inorg. Chem.*, **21**, 3967 (1982).

- [26] J. Dreiser, K.S. Pedersen, A. Schnegg, K. Holldack, J. Nehr Korn, M. Sigrist, P. Tregenna-Piggott, H. Mutka, H. Weihe, V.S. Mironov, J. Bendix, O. Waldmann. *Chem. Eur. J.*, **19**, 3693 (2013).
- [27] (a) M. Srncic, M. Srncic, J. Chalupský, M. Fojta, L. Zendlová, L. Havran, M. Hocek, M. Kývala, L. Rulišek. *J. Am. Chem. Soc.*, **130**, 10947 (2008); (b) E.M.J. Johansson, M. Odelius, S. Plogmaker, M. Gorgoi, S. Svensson, H. Siegbahn, H. Rensmo. *J. Phys. Chem. C*, **114**, 10314 (2010); (c) L. Rulišek. *J. Phys. Chem. C*, **117**, 16871 (2013).
- [28] D.P. Kessissoglou, X.H. Li, W.M. Butler, V.L. Pecoraro. *Inorg. Chem.*, **26**, 2487 (1987).
- [29] C.P. Berlinguette, A. Dragulescu-Andrasi, A. Sieber, J.R. Galán-Mascarós, H.U. Güdel, C. Achim, K.R. Dunbar. *J. Am. Chem. Soc.*, **126**, 6222 (2004).
- [30] C.P. Landee, M.M. Turnbull. *J. Coord. Chem.*, **67**, 375 (2014).
- [31] W. Hiller, J. Strachle, A. Datz, M. Hanack, W.E. Hatfield, L.W. Ter Haar, P. Guetlich. *J. Am. Chem. Soc.*, **106**, 329 (1984).
- [32] (a) L. Jiang, X.L. Feng, T.B. Lu, S. Gao. *Inorg. Chem.*, **45**, 5018 (2006); (b) V. Hoeke, E. Krickemeyer, M. Heidemeier, H. Theil, A. Stammler, H. Bögge, T. Weyhermüller, J. Schnack, T. Glaser. *Eur. J. Inorg. Chem.*, **2013**, 4398 (2013); (c) R.J. Parker, L. Spiccia, B. Moubaraki, K.S. Murray, D.C.R. Hockless, A.D. Rae, A.C. Willis. *Inorg. Chem.*, **41**, 2489 (2002); (d) F. Bonadio, M.-C. Senna, J. Enslin, A. Sieber, A. Neels, H. Stoeckli-Evans, S. Decurtins. *Inorg. Chem.*, **44**, 969 (2005); (e) M. Shatruk, A. Dragulescu-Andrasi, K.E. Chambers, S.A. Stoian, E.L. Bominaar, C. Achim, K.R. Dunbar. *J. Am. Chem. Soc.*, **129**, 6104 (2007).
- [33] (a) C. Yang, Q.L. Wang, Y. Ma, G.T. Tang, D.Z. Liao, S.P. Yan, G.M. Yang, P. Cheng. *Inorg. Chem.*, **49**, 2047 (2010); (b) H. Miyasaka, N. Matsumoto, H. Okawa, N. Re, E. Gallo, C. Floriani. *J. Am. Chem. Soc.*, **118**, 981 (1996); (c) T. Senapati, C. Pichon, R. Ababei, C. Mathoniere, R. Clerac. *Inorg. Chem.*, **51**, 3796 (2012); (d) R. Ababei, Y. Li, O. Roubeau, M. Kalisz, N. Brefuel, C. Coulon, E. Harte, X. Liu, C. Mathoniere, R. Clerac. *New J. Chem.*, **33**, 1237 (2009).
- [34] J.J. Borrás-Almenar, J.M. Clemente-Juan, E. Coronado, B.S. Tsukerblat. *Inorg. Chem.*, **38**, 6081 (1999).
- [35] (a) M. Atanasov, P. Comba, S. Helmle. *Inorg. Chem.*, **51**, 9357 (2012); (b) C. Avendano, F. Karadas, M. Hilfiger, M. Shatruk, K.R. Dunbar. *Inorg. Chem.*, **49**, 583 (2010).
- [36] V. Hoeke, A. Stammler, H. Bögge, J. Schnack, T. Glaser. *Inorg. Chem.*, **53**, 257 (2014).
- [37] (a) H. Oshio, H. Onodera, O. Tamada, H. Mizutani, T. Hikichi, T. Ito. *Chem. Eur. J.*, **6**, 2523 (2000); (b) V. Comte, H. Vahrenkamp. *J. Organomet. Chem.*, **627**, 153 (2001).
- [38] C.A. Bignozzi, S. Roffia, C. Chiorboli, J. Davila, M.T. Indelli, F. Scandola. *Inorg. Chem.*, **28**, 4350 (1989).